Ground layer sensing and compensation

Andrei Tokovinin

Cerro Tololo Inter-American Observatory, Casilla 603, La Serena, Chile

ABSTRACT

A simple analytical method to compute the point spread function for ground-layer compensation at large telescopes is developed. It is shown that a particular form of spatial filtering of high-altitude turbulence achieves very good PSF uniformity and symmetry over a given field. Wave-front sensing with a single low-altitude Rayleigh LGS can reach performance close to optimum at telescopes of medium aperture. Using 4234 real turbulence profiles measured on 21 nights at Cerro Pachón, realistic statistics of ground-layer compensation are computed for the first time. The median FWHM resolution of an AO system with a Rayleigh beacon at 10 km and actuator pitch 0.4 m at 4.2 m telescope is $0\farcs53$, $0\farcs31$, and $0\farcs22$ at 0.5, 0.7, and 1.0 μm wavelength respectively. The median increase of the bightness in the center of stellar image over uncompensated seeing is 1.2, 1.7, and 2.4 magnitudes at those wavelengths.

Keywords: Adaptive optics

1. INTRODUCTION

It is an attractive idea to compensate only near-ground turbulence with adaptive optics.[1–3] The ground layer usually produces most of the image degradation and this degradation is completely isoplanatic. Hence, the benefit of turbulence compensation is achieved in a wide field, unlike the case of classical AO where only a narrow isoplanatic patch near the guide star is compensated. Low-altitude Rayleigh laser beacons (RLGSs) are a natural choice for Ground-Layer Adaptive Optics (GLAO) because they preferentially sense low layers. An RLGS GLAO system is being designed for the 4.2 m SOAR telescope.[4]

Turbulent layers between the ground and the beacons will be compensated, but only partially. The purpose of the analysis presented below is to see how good this compensation can be and what is the effect of the partially compensated layers on the PSF. This will eventually determine the image improvement achievable with GLAO and will set the requirements for the system. The performance of AO systems, including GLAO, is usually studied by Monte-Carlo simulations. Those simulations are computer-intensive, making it difficult or impossible to explore the large space of system parameters. The difficulty is aggravated in the case of Extremely Large Telescopes (ELTs) with apertures of 20 m or more and AO systems of high order. Moreover, simulations are usually done for some average or typical turbulence profile (TP), whereas in reality the TP is highly variable. Using the analytical approach of Rigaut et al.,[5] we develop here a very simple tool for first-order evaluation of the GLAO PSF. Like the uncorrected atmospheric seeing, the resolution of GLAO on large telescopes is independent of aperture size. Telescope aperture is of importance for RLGS because of the cone effect.

2. THE METHOD

Our aim is to compute the long-exposure Point Spread Function (PSF) for GLAO. The residual phase fluctuations in the telescope pupil are Gaussian, hence the long-exposure PSF is directly related to the structure function of the phase residuals $D_\epsilon(\vec{x})$ (in the near-field approximation, neglecting scintillation). Let $T(\vec{k})$ be the long-exposure Optical Transfer Function (OTF) – the Fourier Transform (FT) of the PSF. Then

$$T(\vec{k}) = T_0(\vec{k}) \exp[-0.5 D_\epsilon(\lambda \vec{k})], \quad (1)$$

where $T_0(\vec{k})$ is the OTF of an ideal telescope, λ is the imaging wavelength and $\vec{k}$ is the frequency in image space (in inverse radians).[6] The $T_0(\vec{k})$ term in (1) is responsible for the diffraction-limited core in the compensated

Further author information: E-mail: atokovinin@ctio.noao.edu

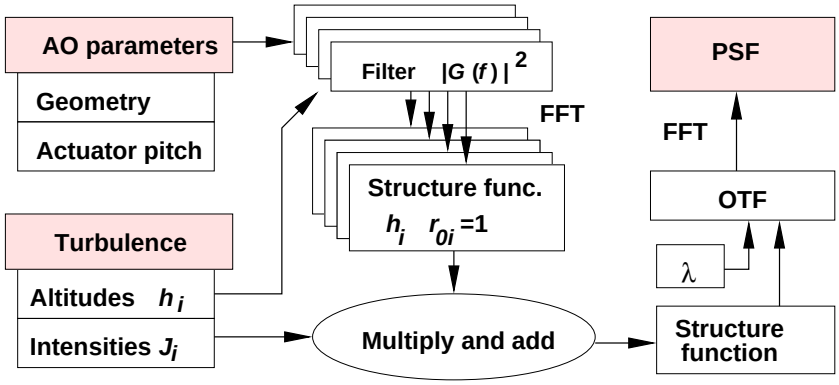

Figure 1. Block-diagram of PSF calculation (see text).

image. For GLAO, the uncompensated turbulence destroys the coherent core and we can put $T_0(\vec{k}) = 1$ for telescope diameter larger than several r_0.

Our approach consists in representing the residual phase by a spatially filtered copy of the atmospheric phase. The spatial filtering typically includes smoothing, shift, and amplitude scaling. Specific forms of this filter depend on the type of AO system and its geometry, and are detailed below for two relevant cases. Thus, the FTs of residual and atmospheric phase are related by some multiplicative factor $G(\vec{f})$. Here $\vec{f}$ is the spatial frequency vector in the pupil plane in m^{-1}. For each layer, the power spectrum of residuals is scaled by $|G(\vec{f},h)|^2$ with respect to the atmospheric phase power spectrum $W_\phi(\vec{f})$:

$$W_\epsilon(\vec{f}) = W_\phi(\vec{f})|G(\vec{f},h)|^2. \tag{2}$$

This is the key point of our analysis. We call $|G(\vec{f},h)|^2$ the *error transfer function* (ETF) because is describes which part of the atmospheric spectrum is left uncorrected by the AO system. The following steps are almost self-evident. First, the power spectrum of residuals is converted into the covariance function $B_\epsilon(\vec{x})$ by FT and the structure function is found as $D_\epsilon(\vec{x}) = 2[B_\epsilon(0) - B_\epsilon(\vec{x})]$. Then the OTF is computed from (1) and converted to a PSF by another FT over $\vec{k}$.

The geometrical factors entering into the filter $|G(\vec{f},h)|^2$ change with the altitude of turbulent layers. As the layers are mutually independent, the resulting power spectrum $W_\epsilon(\vec{f})$ is a sum of the power spectra of all layers. The phase power spectrum of i-th turbulent layer is

$$W_{\phi,i}(f) = 0.0229 f^{-11/3} r_{0,i}^{-5/3}, \tag{3}$$

where $r_{0,i}$ is the Fried radius for layer i, $r_{0,i}^{-5/3} = 0.424(2\pi/\lambda)^2 J_i$, and $J_i = C_n^2 \mathrm{d}h$ is the turbulence integral for that layer in $\mathrm{m}^{1/3}$. The residual power spectrum produced by each layer is a product of $W_{\phi,i}$ and $|G_i(\vec{f},h)|^2$. Summing up the contributions of all layers and passing from power spectrum to structure function, we get the final multi-layer residual structure function D_ϵ as

$$D_\epsilon(\vec{x}) = 0.423(2\pi/\lambda)^2 \sum_{i=1}^{N_{layers}} J_i D_i(\vec{x}), \tag{4}$$

where the structure functions for each layer $D_i(\vec{x})$ are computed from (2) with the corresponding ETF and normalized to $r_{0,i} = 1$.

The set of structure functions D_i depends on the geometry (layer altitudes, viewing directions, actuator pitch), but not on the profile. Thus, it makes sense to pre-compute D_i for some geometry and then to make their linear combinations depending on profile and wavelength. This scheme is illustrated in Fig. 1. The computation in the pupil plane is done on a $N^2 = 128^2$ grid with a 0.05 m step. The total grid size is thus

$L = 6.4$ m, assuring fine PSF sampling of λ/L. To increase the accuracy of structure-function calculation, the grid in $\vec{f}$-space is made with 4 times finer step, but only the central part of the resulting $(4N)^2$ spatial grid is then used. We checked that the FWHM of uncompensated images computed by this technique closely matches the known formula.

The limitations of this approach are obvious. The temporal response of closed-loop AO system and sensor noise are neglected. The fact that tip-tilt signal for LGS beacons is derived from off-axis NGS is ignored, although it probably could be included by modifying the ETF. At infra-red wavelengths, the residual structure function may saturate at a level below ~ 3 rad^2, in which case we can no longer neglect the aperture cutoff $T_0(\vec{k})$. It is trivial to include the effect of outer scale. Despite its limitations, the model should provide adequate first-order estimates of GLAO performance at short wavelengths. Now the ETFs for two specific cases will be given.

2.1. Optimum compensation

We start with an idealization: supposing that the instantaneous perturbations in the whole atmospheric volume are known, how well can they be corrected by a single DM over a finite field? This situation is a specific case of correction with several DMs considered in Ref. 7. Let h_m be the conjugation altitude of the DM. According to Ref. 7, the appropriate ETF for a layer at altitude h is

$$|G(\vec{f},h)|^2 = 1 - 2g(f,h)r(f)\cos[2\pi(\vec{f}\vec{\theta})(h-h_m)] + g^2(f)r^2(f). \quad (5)$$

Here the spatial filter $g(f,h)$ that we apply to a given turbulent layer for best correction is constrained to be circular-symmetric in order to avoid any asymmetry around the center of the field. An additional filter $r(f)$ is introduced to represent a finite compensation order. In the following, we adopt a simple low-pass filter: $r(f) = 1$ for $f < 2/d_{act}$ and $r(f) = 0$ elsewhere, d_{act} being the actuator spacing (or pitch).

If $|G(\vec{f},h)|^2$ is averaged over the direction of $\vec{\theta}$ (i.e. over a circle of radius θ_0 in the image space), the filter $g(f,h)$ that minimizes the residual phase variance at this radius is found[7] to be the Bessel function, $g(f,h) = J_0[2\pi f\theta_0(h-h_m)]/r(f)$.

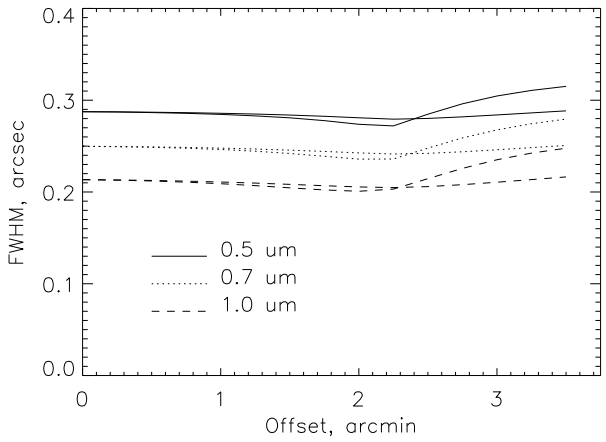

Figure 2. The FWHM of GLAO-compensated PSF for Gemini-Pachón turbulence profile at three wavelengths. The pairs of curves show the FWHM in longitudinal and transverse directions to evaluate the PSF symmetry. Actuator pitch 0.2 m, field optimization for $\theta_0 = 2.5'$.

With this Bessel filter, the best correction is achieved near the edge of the field. Surprizingly, the PSF variation over the whole field is very small. For $\theta > \theta_0$ the correction degrades and the PSF becomes asymmetric (Fig. 2). This result is unexpected: a filter that minimizes the rms residual at the edge of the field turns out, at the same time, to produce PSF with very good uniformity and symmetry over the whole field!

Is the Bessel filter the best one in terms of the PSF uniformity? If we average the ETF over the whole field of view (i.e. over the entire circle instead of a ring), the form of the optimum filter will change to the Airy function, $g(f,h) = J_1[2\pi f\theta_0(h-h_m)]/[\pi f\theta_0(h-h_m)]$. This filter *does not* give such good PSF uniformity. Rigaut[1] suggested a sinc filter (1-dimensional) that is also worse than the Bessel filter.

The optimum smoothing of individual turbulent layers found here consists in averaging each layer over a ring of radius $\theta_0(h - h_m)$. This can be achieved by sensing wave-fronts from a large number of stars located on the sky on a circle of radius θ_0 and averaging the signals. Of course, no such constellation exist on the sky. However, several sodium LGSs placed in a ring at the edge of the field[1] provide a very good approximation.

2.2. Turbulence compensation with a Rayleigh beacon

We presume that both wave-front sensing and compensation is done at the ground level and consider one thin turbulent layer at the altitude h above the ground. The beacon's altitude is H. The angular distance between the beacon and the object changes across the telescope pupil. Let $\vec{\theta}$ be the beacon-object angle as viewed from the center of the aperture, and $\vec{y}$ – the coordinate vector in the aperture plane. The beacon is assumed to be on the optical axis of the telescope. From the simple geometry, the relative shift $\vec{b}$ between object and beacon wave-fronts viewed from the point $\vec{y}$ in the aperture is

$$\vec{b} = \vec{y}\frac{h}{H} + \vec{\theta}h \tag{6}$$

The beam from the object (at infinity) is cylindrical, whereas the beacon's beam is conical. Because of this, the part of the turbulent layer sampled by the beacon is $\alpha = 1 - h/H$ times smaller than that sampled by the object. Consequently, the aberrations as sensed by RLGS are reduced α times with respect to the aberrations from the object. It is this reduction that leads to preferential sensing of the lowest layers. For turbulent layers lying above the laser beacon, $h > H$, we put $\alpha = 0$, which means no turbulence compensation. In fact some partial compensation of the tilt produced by high turbulent layers is possible because the light of tip-tilt NGS samples those layers. In this study we neglect this small effect.

A complication arises here because the differential wave-front "stretching" between object and beacon precludes the use of standard Fourier-analysis techniques. In other words, the relative shift between the wave-fronts $\vec{b}$ depends on the coordinate in the pupil $\vec{y}$. If the relevant scale (i.e. the coherence scale r_0) is much less than the size of telescope aperture, however, we may consider the shift $\vec{b}$ as approximately constant over a given part of the aperture, thus neglecting the "stretching". The resulting OTF is computed from the aperture-averaged structure function – an approximation used in many AO-related studies.[8]

The compensating phase is derived from the atmospheric phase shifted by $\vec{b}$, reduced α times and smoothed by the spatial response of the DM $r(f)$. Hence the ETF for a given part of the telescope aperture is

$$|G(\vec{f},h)|^2 = |1 - \alpha r(\vec{f})\exp[-2\pi i(\vec{f}\,\vec{b})]\,|^2 = 1 - 2\alpha r(\vec{f})\cos[2\pi(\vec{f}\vec{b})] + \alpha^2 r^2(\vec{f}). \tag{7}$$

We use (6), separate the part containing $\vec{y}$ from the cosine and average it spatially over aperture – a circle of diameter D. The result is the Airy function $A(f,h) = 2J_1(\pi f D h/H)/[\pi f D h/H]$. The final expression for the aperture-averaged ETF is

$$|\overline{G}(\vec{f},h)|^2 = 1 - 2\alpha r(f)A(f,h)\cos[2\pi h(\vec{f}\vec{\theta})] + \alpha^2 r^2(f). \tag{8}$$

3. TWO GLAO SYSTEMS

We test the formalism developed in the previous Section on two examples, presented schematically in Fig. 3 and denoted as systems A and B in the following.

System A is an optimized compensation with a DM conjugated to the ground. The field radius $\theta_0 = 1.5'$ is chosen. At a distance of 10 km, it selects a ring of 4.4 m radius on the wave-front. Thus, only large-scale perturbations will be compensated in high turbulent layers, whereas for the ground layer the degree of compensation is set by the actuator pitch, typically $d_{act} = 0.4$ m for the examples considered below. The transition between the DM-limited and field-limited regimes occurs at an altitude of $d_{act}/\theta_0 = 1$ km. All layers below 1 km will be compensated almost equally, hence there is no need to know the TP with altitude resolution

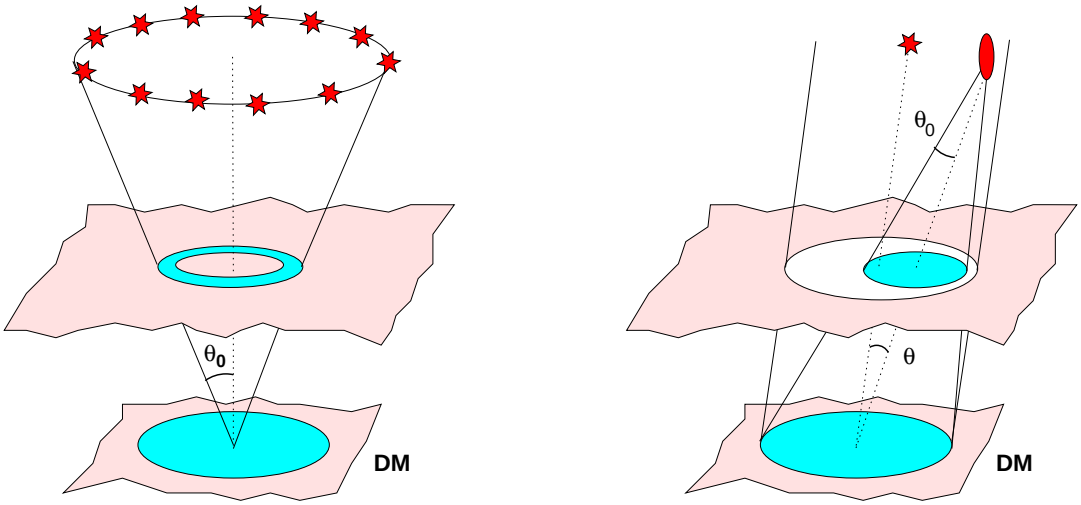

Figure 3. Two cases considered here: optimized compensation (system A, left) and RLGS (system B, right).

much better than 1 km for evaluating the performance of system A. The results do not depend on the telescope aperture diameter as long as it is sufficiently large.

Can a ring of sodium LGSs approximate the optimized compensation? The answer depends on the relation between the shifts across telescope aperture caused by the finite distance to LGS, hD/H, and the size of averaging kernel needed for optimized compensation, $\theta_0 h$. For a good approximation we require that the shifts be small, or $D < \theta_0 H$. For $H = 90$ km and $\theta_0 = 1.5'$ this translates to $D < 39$ m. Thus, sodium LGSs are a good approximation to system A even for ELTs.

System B uses a RLGS beacon at an altitude of $H = 10$ km above ground, with the DM conjugated to the ground. Here, the smoothing of high-altitude turbulent layers is achieved by the variable shifts between object and LGS wave-fronts over the aperture. The characteristic field angle where this averaging will be effective is of the order of $\theta_0 = 2H/D$, where D is the telescope diameter. With increasing D, the shifts become larger and compensation order lower, whereas the diameter of the compensated field increases. We select $D = 4.2$ m and $d_{act} = 0.4$ m to match the proposed GLAO system for SOAR telescope.[4]

The **figures of merit** for GLAO performance are the Full Width at Half Maximum (FWHM) of the compensated PSF (in two directions to assess the symmetry) and the Strehl gain, i.e. the increase of the central intensity of the PSF expressed in magnitudes. The Strehl gain is useful for evaluating the increase of light flux in a small aperture, e.g. for imaging spectrometers, for background-limited detection and spectroscopy of faint objects, and for photometry in crowded fields.

The FWHM of the compensated PSF is to be compared to the FWHM of the seeing-limited PSF in a large telescope (or "seeing") $\beta = 0.98\lambda/r_0$. A useful formula to compute the seeing in arcseconds for 0.5 μm wavelength at zenith from the total turbulence integral J_{tot} in $\mathrm{m}^{1/3}$ is $\beta = (J_{tot}/6.8 \cdot 10^{-13})^{0.6}$. The *free-atmosphere seeing* β_f is defined as the seeing produced by all layers above a certain level, taken here to be 0.5 km. Naively, one might expect that GLAO would produce the FWHM of the order of β_f. In reality the ground layer is not fully compensated, but, on the other hand, higher layers get some degree of compensation. Thus, the GLAO FWHM can be both larger and smaller than β_f.

4. GEMINI-PACHÓN TURBULENCE PROFILE MODEL

Turbulence profiles at Cerro Pachón were measured in 1998 during the Gemini site characterization campaign.[9] A 7-layer representation of the average TP suggested in Ref. 10 has been used in many studies on AO and became a *de facto* standard model. The total seeing is $\beta = 0''.67$ ($r_0 = 0.15$ m at 0.5 μm wavelength). Ground layer contains 65% of turbulent energy, so $\beta_f = \beta(1 - 0.65)^{0.6} = 0''.36$.

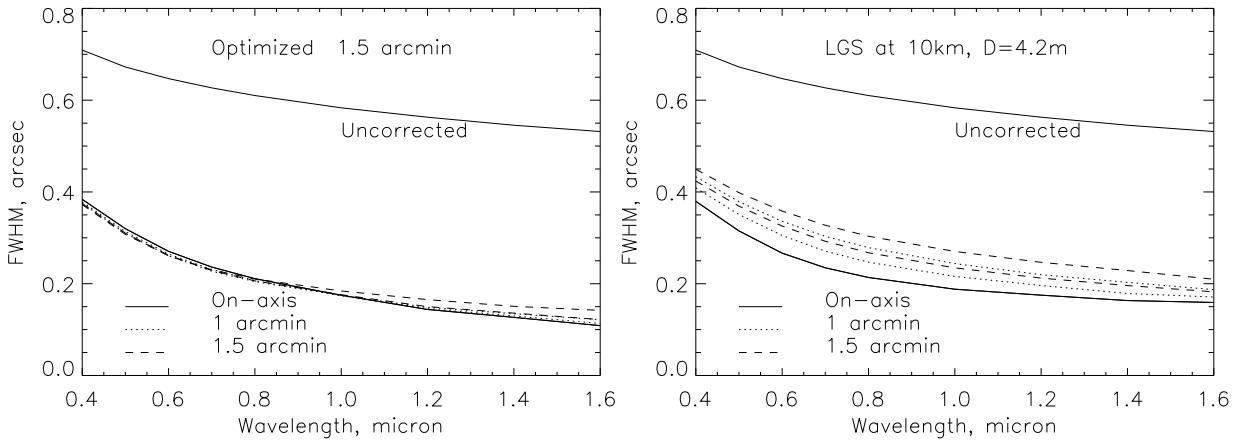

Figure 4. The FWHM for the optimized compensation (system A, left) and RLGS (system B, right) with Gemini-Pachón turbulence profile as a function of wavelength. The pairs of curves show the FWHM in orthogonal directions.

In Fig. 4, a detailed comparison of FWHM resolution for optimized and RLGS cases is presented. It is clear that optimized compensation provides a very good PSF uniformity and symmetry – better than could be achieved with RLGS. On the other hand, the overall gain over un-compensated PSF in both cases is comparable. The results obtained here closely match calculations of RLGS GLAO system for the SOAR 4.2 m telescope done previously with the modal covariance code[4] using the same TP. Good agreement is found with the results of Chun[2] who also used this TP model.

We evaluated the performance of the RLGS for telescopes of increasing aperture. As expected, with increasing aperture the compensation quality is lower, but the PSF symmetry and uniformity are improved. For $D = 32$ m the FWHM closely matches β_f: the cone effect is so large that all layers except the ground layer are uncorrected. In this case, the results are sensitive to the presence of layers in the first kilometer above the ground (no such layers in the Gemini-Pachón model). Generally, TPs with a resolution of d_{act}/θ_0 at low altitudes are required for reliable estimates of GLAO performance. On the other hand, as high layers remain un-compensated, only their total intensity matters and a TP measurement with low resolution at high altitudes will be adequate.

5. REAL TURBULENCE PROFILES AT CERRO PACHÓN

In January 2003, low-resolution turbulence profiles were measured at Cerro Pachón with the MASS instrument.[11] Simultaneously, the total seeing was measured by a differential image motion monitor, DIMM (installed at 1.5 m above ground), which permitted calculating the intensity of ground layer by subtraction. The observations were performed by J. Vasquez on 21 nights from January 8 to January 31, 2003. All nights were clear. MASS measured TPs every minute, some 400 profiles per night. There were nights with quite calm upper atmosphere during this period. The nightly average of β_f was below $0\farcs4$ on 10 nights out of 21, with a record of $0\farcs205$ on January 15/16, 2003. Extensive study of TP with MASS at neighboring Cerro Tololo is also available.[12]

The total of 4234 profiles were grouped in quartiles of the β_f distribution. In the following we call those groups good, fair, poor, and bad. The median and average layer intensities in each group are plotted in Fig. 5. It is evident that the variations of β_f are caused by turbulence at intermediate altitudes: the highest layer is almost constant, producing a seeing of $0\farcs15$. The ground layer (likely over-estimated by low-altitude DIMM) also does not show any correlation with β_f and dominates the total seeing of about $1''$.

In Fig. 6 the Strehl gain is plotted as a function of wavelength and actuator pitch for systems A and B. As expected, the largest GLAO gain is achieved in good conditions. In this case the actuator pitch is critical in the visible range because ground-layer turbulence is rather strong. It becomes less important for reduced ground-layer strength. On the other hand, actuator pitch is of little importance in the case of strong high-altitude

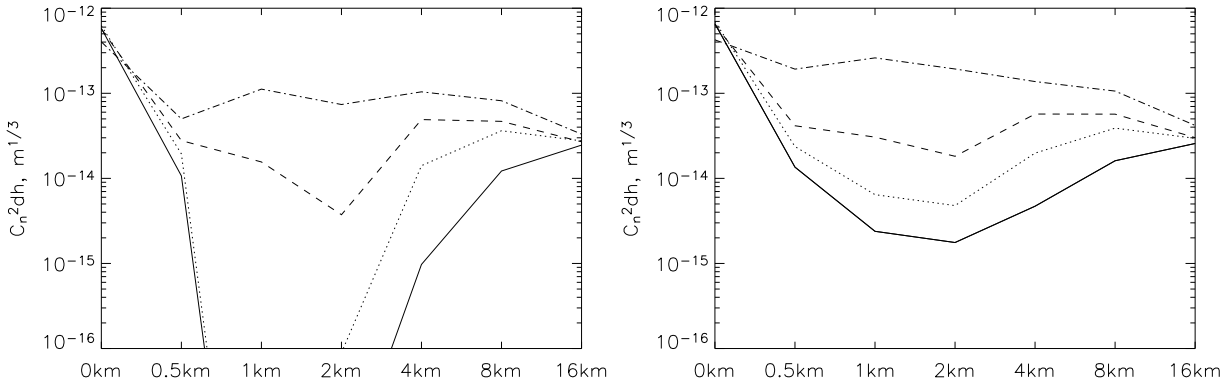

Figure 5. Turbulence profiles at Cerro Pachón in January 2003. Full, dotted, dashed and dot-dashed lines show the median (left) and average (right) profiles grouped in the good, fair, poor and bad free-atmosphere seeing. The corresponding median β_f for each group are 0.″245, 0.″356, 0.″518, and 0.″90. Horizontal axis – altitudes above mountain in km, vertical axis – integrals over the layers in $m^{1/3}$.

turbulent layers (Fig. 6, right) where the correction order of high layers is set by spatial filtering rather than by the DM actuators.

Is the low resolution of the TPs delivered by MASS adequate for GLAO studies? The intensities of turbulent layers are measured by MASS correctly, but the layers are poorly localized within thick "slabs" with predefined logarithmically-spaced altitudes. To answer this question, we artificially distorted the altitudes of layers multiplying them by $2^{\zeta-0.5}$, where ζ is a random number uniformly distributed between 0 and 1. The computation of GLAO performance for system B was repeated for 9 random distortions of altitude grid, for 4 median TPs discussed above and for 3 wavelengths. The rms difference between distorted and un-distorted Strehl gains for all $4 \cdot 3 \cdot 9 = 108$ cases is only 0.027^m, with no systematic shift and maximum deviations of $(-0.05^m, +0.15^m)$. Thus, MASS resolution is adequate for this study.

Perhaps surprisingly, systems A and B show comparable GLAO performance. The Strehl gains for system B are lower under good conditions and higher under poor conditions. The difference in performance is small compared to the simplicity and cost advantages of RLGS over sodium lasers. This is understandable: in good

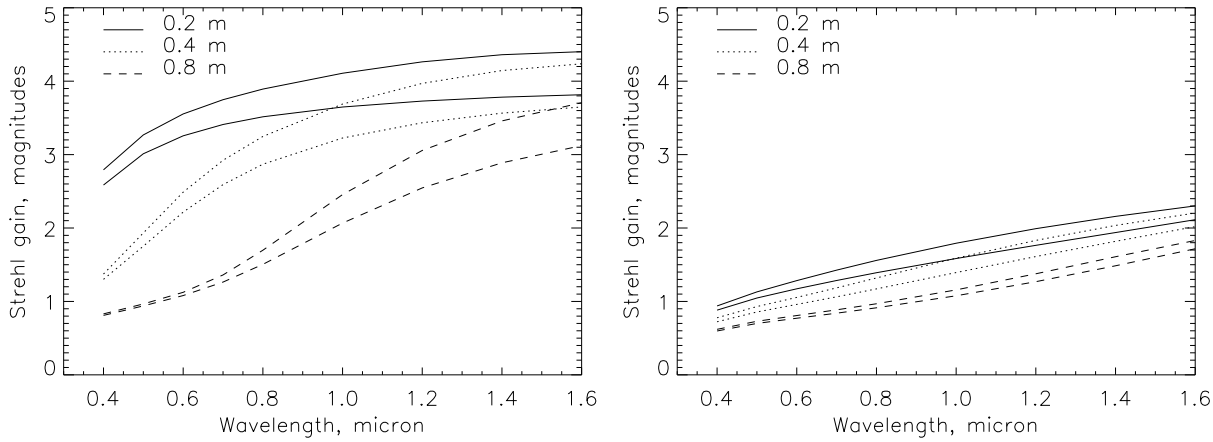

Figure 6. Gain in on-axis Strehl ratio as a function of imaging wavelength for good (left) and bad (right) median Pachón profiles (total seeing 0.″95 and 1.″15) for two GLAO systems. The full, dotted and dashed lines correspond to actuator pitch of 0.2, 0.4, and 0.8 m. On the left plot, the curves for system A are above those for system B, on the right plot it is the opposite.

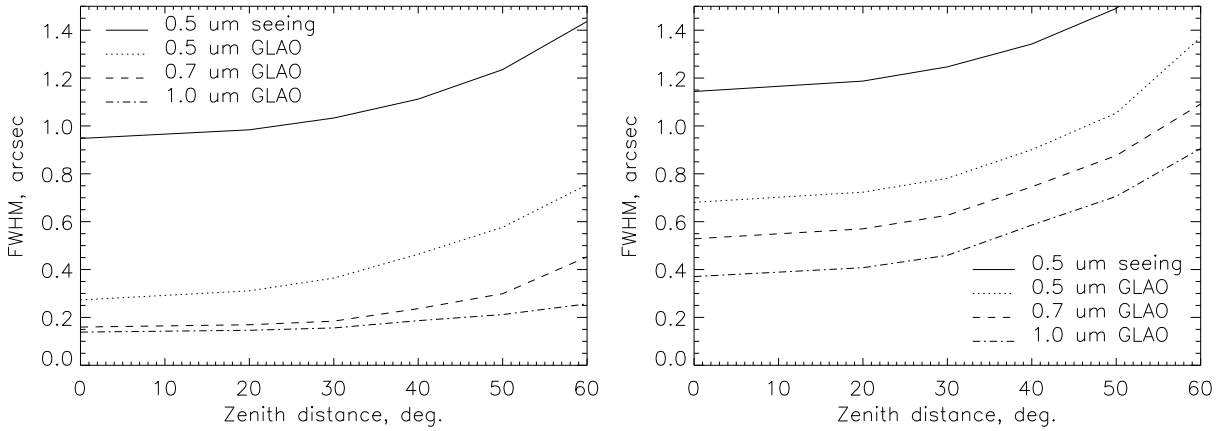

Figure 7. Dependence of FWHM for system B on zenith distance of observation for good (left) and bad (right) median turbulence profiles. Uncorrected seeing at 0.5 μm is plotted in full line.

conditions, the ground layer is well sensed by the RLGS. A non-negligible gain is still achieved even for poor conditions, which means that GLAO will be useful more than 50% of time. This conclusion may be slightly optimistic because it is based on turbulence statistics over a good and stable month of the year.

So far, it was implicitly assumed that the observations are done at zenith. When this is not the case, two effects intervene: first, the altitudes of the layers are increased as $\sec z$ and, second, the turbulent integrals are increased in the same proportion. Both effects can be incorporated into the pre-calculated structure functions. In Fig. 7 the zenith-angle dependence of corrected and un-corrected FWHM is plotted for good and bad median TPs. Although the gain brought by GLAO remains significant even away from zenith, is is strongly recommended to observe as close to zenith as possible.

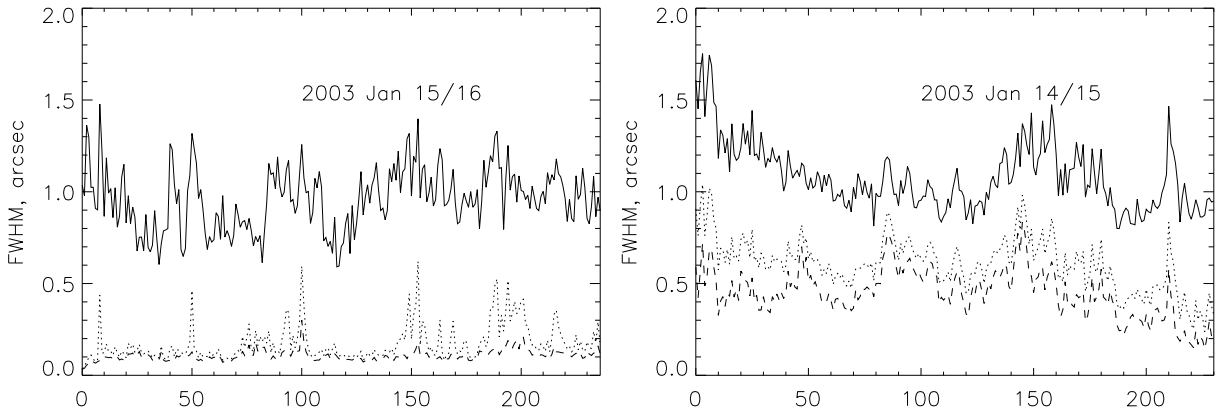

Figure 8. Evolution of total seeing (full line) and GLAO-compensated seeing at 0.5 μm (dotted) and 0.7 μm (dashed) for system B. The sequential profile number is plotted on the horizontal axis. The nights selected correspond to good and bad β_f.

Now we address the statistics of GLAO gains for system B using individual profiles. It should be stressed that a significantly better performance at 0.5 μm would be obtained with smaller actuator pitch – at increased cost of the AO instrument, of course.

The PSF at three representative wavelengths was computed for all 4234 turbulence profiles. In Fig. 8 the temporal evolution of image FWHM is shown for two nights that span a range of conditions. The night of January 15/16 was exceptional, with resolution at 0.7 μm approaching $0\farcs1$. In Fig. 9 the cumulative histograms

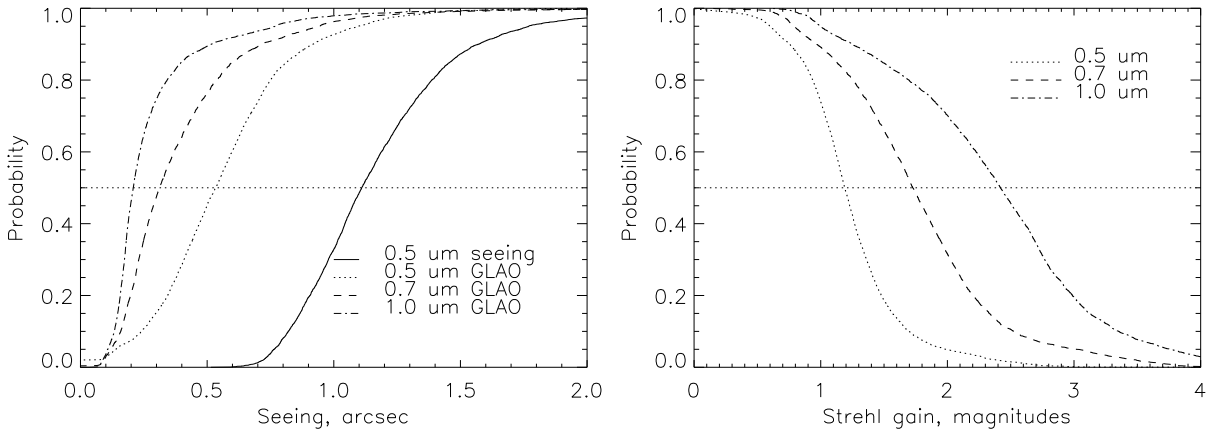

Figure 9. Cumulative histograms of FWHM (left) and Strehl gain (right) for system B based on the full set of 4234 turbulence profiles measured at Cerro Pachón in January 2003. It is likely that the uncorrected seeing was over-estimated because of the low altitude of DIMM above ground.

Table 1. Statistics of GLAO gain for system B

Parameter	Best 25%	Median	75%
Seeing β, arcsec	0.94	1.11	1.33
β_f, arcsec	0.30	0.42	0.65
FWHM at 0.5 μm, arcsec	0.38	0.53	0.71
FWHM at 0.7 μm, arcsec	0.22	0.31	0.49
FWHM at 1.0 μm, arcsec	0.17	0.22	0.30
Strehl gain at 0.5 μm, mag.	1.41	1.19	0.99
Strehl gain at 0.7 μm, mag.	2.11	1.73	1.36
Strehl gain at 1.0 μm, mag.	2.87	2.42	1.88

for all profiles are plotted, both for FWHM and for Strehl gains. The histogram of β_f is not plotted, it is somewhere in-between the GLAO curves for 0.5 and 0.7 μm. The representative histogram levels are given in Table 1.

6. CONCLUSIONS

A first-order analysis for predicting the performance of GLAO is developed here. When applied to the "standard" Gemini-Pachón TP, it gives a good agreement with other published results. The simplicity of the model permits us to explore a wide range of system parameters without recourse to costly Monte-Carlo simulations.

It is shown that the optimized compensation scheme with the Bessel filter leads to high PSF uniformity and symmetry over the field. Optimized compensation could be implemented with several sodium LGS located in a ring around the field. On the other hand, a low-altitude RLGS offers similar gains over natural seeing at somewhat less uniform compensation over the field.

For the first time, we have computed the GLAO performance for a large set of real TPs measured at Cerro Pachón in January 2003. The evolution of GLAO-compensated PSF over the time is shown for some representative nights, and full statistics of the GLAO performance are given. Even with an actuator pitch too coarse to fully compensate the $1''$ ground-layer seeing in the visible, the gain from GLAO is significant. Importantly, the gain is present on all nights, even on bad ones. In the red and near-IR parts of the spectrum where the adopted actuator pitch is adequate, the resolution gain from GLAO becomes *very* significant: on 25% of nights the FWHM of compensated images reaches $0\farcs2$.

Our further plan is to consider the case of several LGSs and to develop a GLAO concept for ELTs based on multiple RLGSs.

ACKNOWLEDGMENTS

The work of J. Vasquez and other colleagues who prepared and executed the MASS campaign at Cerro Pachón is acknowledged. I am grateful to B. Gregory and S. Heathcote for discussions and comments.

REFERENCES

1. F. Rigaut, "Ground Conjugate Wide Field Adaptive Optics for the ELTs," in: *Beyond Conventional Adaptive Optics,* eds. E. Vernet, R. Ragazzoni, S. Esposito, N. Hubin, ESO Conf. Workshop Proc. **58**, ESO, Garching bei München, p. 11-17, 2002
2. M. Chun, "Gains from ground-only adaptive optics system", Proc. SPIE, **4839**, pp. 94-98, 2003
3. R.G.M. Rutten, P. Clark, R.M. Myers et al., "Facility class Rayleigh beacon AO system for the 4.2m William Hershel Telescope," Proc. SPIE, **4839**, pp. 360-369, 2003
4. A. Tokovinin, B. Gregory, H. Schwarz, V. Terebizh, and S. Thomas, "A visible-light AO system for the 4.2 m SOAR telescope", Proc. SPIE, **4839**, pp. 673-680, 2003
5. F. Rigaut, J.-P. Véran, and O. Lai, "An analytical model for Shack-Hartmann-based adaptive optics systems", in *Adaptive Optical System technologies,* D. Bonaccini, ed., Proc. SPIE, **3353,** pp. 1038-1048, 1998
6. F. Roddier, "The effects of atmospheric turbulence in optical astronomy," in *Progress in Optics*, E. Wolf, ed., **19**, pp. 281-376, North-Holland, Amsterdam, 1981.
7. A. Tokovinin, M. Le Louarn, and M. Sarazin, "Isoplanatism in a multi-conjugate adaptive optics system", JOSA(A), **17**, pp. 1819-1827, 2000
8. J.-P. Véran, F. Rigaut, H. Maître, and D. Rouan , "Estimation of the adaptive optics long-exposure point-spread function using control loop data," JOSA(A), **A14**, pp. 3057-3069, 1997
9. J. Vernin, A. Agabi, R. Avila, M. Azouit, R. Conan, F. Martin, E. Masciadri, L. Sanchez, and A. Ziad, "Gemini site testing campaign. Cerro Pachon and Cerro Tololo," *Gemini RPT-AO-G0094*, `http://www.gemini.edu/`, 2000
10. B. L. Ellerbroek and F. Rigaut, "Scaling Multi-Conjugate Adaptive Optics Performance Estimates to Extremely Large Telescopes," in *Adaptive Optical Systems Technology,* P. L. Wizinovich, ed., Proc. SPIE, **4007**, pp. 1088-1099, 2000
11. V. Kornilov, A. Tokovinin, O. Voziakova, A. Zaitsev, N. Shatsky, S. Potanin, and M. Sarazin, "MASS: a monitor of the vertical turbulence distribution," Proc. SPIE, **4839**, pp. 837-845, 2003
12. A. Tokovinin, S. Baumont, J. Vasquez, "Statistics of turbulence profile at Cerro Tololo," MNRAS, **340**, pp. 52-58, 2003